Original Article

The value of contrast-enhanced ultrasound fusion imaging in percutaneous liver biopsy for liver lesions invisible on conventional B-mode ultrasound

Yuhong He^, Li Gong^, Jie Wu^, Baojie Wen^, Wentao Kong^

Department of Ultrasound Medicine, Nanjing Drum Tower Hospital, Affiliated Hospital of Medical School, Nanjing University, Nanjing, China

Contributions: (I) Conception and design: W Kong, Y He; (II) Administrative support: W Kong; (III) Provision of study materials or patients: L Gong, B Wen, J Wu; (IV) Collection and assembly of data: Y He, J Wu, L Gong, B Wen; (V) Data analysis and interpretation: W Kong, Y He; (VI) Manuscript writing: All authors; (VII) Final approval of manuscript: All authors.

Correspondence to: Wentao Kong, PhD. Department of Ultrasound Medicine, Nanjing Drum Tower Hospital, Affiliated Hospital of Medical School, Nanjing University, No. 321 Zhongshan Street, Nanjing 210009, China. Email: breezewen@163.com.

Background: Ultrasound (US) is the most commonly used imaging method for guiding percutaneous liver biopsies. For lesions that are invisible on B-mode ultrasound (BMUS), contrast-enhanced ultrasound (CEUS) improves the contrast between neoplasms and liver parenchyma, while emerging fusion imaging techniques can enhance the localization of lesions. Therefore, our study aimed to assess the value of CEUS fusion imaging in detecting and guiding percutaneous liver biopsy for lesions invisible on BMUS.

Methods: Patients with focal liver lesions (FLLs) identified on computed tomography (CT) or magnetic resonance imaging (MRI) but not visible on BMUS were retrospectively included at Nanjing Drum Tower Hospital, Affiliated Hospital of Medical School, Nanjing University from September 2019 to December 2023. All patients underwent BMUS fusion imaging and CEUS fusion imaging. We evaluated the lesion visibility, detection rate of BMUS fusion, and CEUS fusion before liver biopsy and the rate of technical success and diagnostic success after CEUS fusion-guided biopsy.

Results: This study included 70 FLLs from 61 patients. The mean visibility score of the 70 lesions on BMUS was 1.51±0.52. BMUS fusion detected 31 (31/70, 44.3%) lesions, yielding a mean visibility score of 1.81±1.03. CEUS fusion detected 63 (63/70, 90%) lesions, and achieved a mean visibility score of 2.90±0.30, which was significantly higher than that of BMUS fusion. Subgroup analysis corroborated the superiority of CEUS fusion in detecting infiltrative lesions and lesions <2 cm. Finally, CEUS fusion-guided liver biopsy achieved a technical success rate of 98.4% and a diagnostic success rate of 82.0% (50/61).

Conclusions: Compared with conventional BMUS or BMUS fusion imaging, the combination of CEUS and fusion imaging enabled an increase in the detection rate and lesion visibility of BMUS-invisible lesions, particularly for infiltrative masses and small-sized lesions, thereby increasing operators' confidence and success rate during the percutaneous liver biopsy.

Keywords: Fusion imaging; contrast-enhanced ultrasound (CEUS); percutaneous liver biopsy; focal liver lesion (FLL); hepatocellular carcinoma (HCC)

Submitted Jun 02, 2024. Accepted for publication Dec 23, 2024. Published online Jan 22, 2025.
doi: 10.21037/qims-24-1104
View this article at: https://dx.doi.org/10.21037/qims-24-1104

^ ORCID: Wentao Kong, 0000-0002-4313-6958; Yuhong He, 0009-0003-9676-1006; Li Gong, 0000-0001-7006-8658; Jie Wu, 0000-0002-3483-7736; Baojie Wen, 0000-0001-5692-7057.

Introduction

In recent years, with the development of multiple imaging modalities including computed tomography (CT), magnetic resonance imaging (MRI), and positron emission tomography-CT (PET/CT), the detection of focal liver lesion (FLL) has significantly improved. In turn, this has increased the requirement for percutaneous liver biopsy (PLB), which is the gold standard of diagnosis and the cornerstone of therapy for patients with FLLs (1-4). As the most commonly used image guidance for the PLB, ultrasound (US) is a real-time, accessible, nonradioactive, and affordable modality (5,6). Apart from the experience of the operator, the success rate of PLB also depends largely on the accurate targeting of FLLs, which can increase operators' confidence and prevent the need for a second biopsy or false-negative results.

An inherent limitation of conventional B-mode US (BMUS), apart from its single-acoustic window, is the poor conspicuity of several FLLs in obese patients or that arising due to bowel gas/rib echo, which can lead to a lost opportunity to complete US-guided PLB or other minimally invasive interventional therapies (7). Although CT and MRI offer better resolution for soft tissue, the radiation, high cost, and possibility of renal affection and allergic reactions limit their use in imaging guidance for interventional procedures (8,9).

With the widespread use of US agents such as SonoVue (Bracco, Italy) and Sonazoid (GE Healthcare, Chicago, IL, USA), contrast-enhanced ultrasound (CEUS) has significantly contributed to the detection and diagnosis of FLLs that are poorly visualized on BMUS via the increase in the contrast ratio of blood vessels and liver parenchyma (10,11). For instance, CEUS-guided PLB with radiofrequency ablation (RFA) has achieved considerable technical success, with high sensitivity and specificity (12-15). The various enhancement patterns of CEUS allow for the viable portion of the tumor to be distinguished from the necrotic area, thus reducing the rate of false-negative results.

In facilitating the acquisition of multi-image information for physicians, the development of volume navigation and multiplanar reconstruction techniques allows for two-dimensional CT/MRI images and US images to be displayed in the same plane through registration based on vital anatomical marks. Fusion imaging improves the localization of target lesions that are indiscernible on BMUS due to the small size or specific localization (16,17), and its value in image guidance for PLB and RFA has been demonstrated in several studies (18-22).

Although both CEUS and fusion imaging can serve as imaging guidance for interventional therapies alone, they are each associated with certain limitations. For instance, in Lim *et al.*'s study, although the target hepatic lesion was clearly visualized on fusion imaging, there was still a chance of inaccurate localization of the target lesion during the biopsy procedure or RFA (23). Moreover, it has been reported that CEUS involves detection limits for deep lesion, hypovascular hepatocellular carcinoma (HCC) in a cirrhotic background and lesions near the subphrenic regions (24). Hence, CEUS should be performed for lesions that are invisible on fusion imaging. Our study thus aimed to compare the values BMUS-CT/MRI fusion imaging and that of CEUS-CT/MRI fusion imaging in PLB for FLLs that are invisible on BMUS. We present this article in accordance with the STROBE reporting checklist (available at https://qims.amegroups.com/article/view/10.21037/qims-24-1104/rc).

Methods

Patients

From September 2019 to December 2023, 736 patients with suspected FLLs from CT/MRI were referred to the Department of Ultrasound Medicine, Nanjing Drum Tower Hospital, Affiliated Hospital of Medical School, Nanjing University, to undergo PLB for confirmation of the diagnosis. The selection of image guidance for the biopsy procedure was decided upon by experienced operators as follows: (I) biopsy was performed under BMUS guidance only if the target lesion was sufficiently visible on BMUS. (II) If the lesion was not clearly visible and had a blurred boundary or if its echogram was insufficiently typical for localization on BMUS, further BMUS-CT/MRI fusion imaging was performed to improve the visualization of the target lesion. (III) CEUS-CT/MRI fusion imaging was performed to optimize the lesion localization if the target lesion remained unremarkable on BMUS-CT/MRI fusion imaging.

The inclusion criteria were as follows: (I) FLLs were detected by CT or MRI; (II) FLLs were invisible or had an inconspicuous margin on BMUS; (III) FLLs could be visualized on BMUS but had an echogram not sufficiently typical for localization of the target lesion, such as an unclear boundary between target tumors and hyperechoic

nodules in the cirrhosis background; and (IV) patients received both BMUS fusion and CEUS fusion imaging.

The exclusion criteria were as follows: (I) lesions visible on BMUS and with sufficient visibility for guidance of the PLB; (II) lesions located in a sonographically blind area (e.g., subphrenic area of the right liver); (III) obvious bleeding tendency, severe thrombopenia, or coagulation disorders [prothrombin time activity <50%, international normalized ratio (INR) >1.7, blood platelet count $<50\times10^9$/L]; (IV) uncooperative patients; and (V) patients with contraindications to CEUS.

This study was conducted in accordance with the Declaration of Helsinki (as revised in 2013) and study was approved by the Institutional Ethics Committee of the Nanjing Drum Tower Hospital, Affiliated Hospital of Medical School, Nanjing University (No. 2022-140-01). Informed consent were obtained from all patients prior to biopsy.

Baseline characteristics

The baseline characteristics of all enrolled patients were collected, including gender, age, history of hepatitis, history of liver cirrhosis, history of tumor, and tumor markers (alpha-fetoprotein, carcinoembryonic antigen, carbohydrate antigen 125, carbohydrate antigen 199). The baseline characteristics of the target lesions, including size, localization, count, and final diagnosis, were also recorded.

Imaging equipment and reagents

The LOGIQ E9 system (performed with a 1–6 MHz convex probe; GE Healthcare) equipped with a real-time volume navigation system was used for US imaging and fusion imaging, which consisted of a magnetic field generator near the patient, and a tiny magnetic sensor attached to the US transducer. The magnetic field generator transmitted an alternating magnetic field and built up a three-dimensional (3D) spatial coordinate system around itself. The identity and direction detected by the magnetic sensor were then used to calculate the location and direction of the spatial coordinates. Both the magnetic field generator and the sensor were connected to a fully integrated magnetic tracking system embedded in the US machine. The contrast agents SonoVue (Bracco) and Sonazoid (GE Healthcare) were used for CEUS examination. Biopsy was performed with a disposable 18-gauge automated biopsy needle (Marquee, BD, Franklin Lakes, NJ, USA).

A 3.0-T MRI system (Ingenia 3.0T/Ingenia CX 3.0T, Philips Healthcare, Best, The Netherlands) was used for the MRI examination. Unenhanced, arterial-phase, portal-phase, and equilibrium-phase images were acquired using a 3D T1-weighted sequence with a multi-echo Dixon fat-water separation technique. A dose of 0.025 mmol/kg of Gd-EOB-DTPA (Primovist, Bayer, Leverkusen, Germany) or 0.1 mmol/kg of Gd-DTPA-BMA (Omniscan, GE HealthCare) was administered as an intravenous bolus. Patients imaged with Gd-EOBDTPA were additionally imaged in the hepatobiliary phase (HBP) after 20 minutes.

CT examinations were performed with a multidetector CT scanner (Revolution CT/Revolution Maxima; GE HealthCare) with a slice thickness of 1.25 mm. Hepatic arterial-, portal venous-, and equilibrium-phase images were obtained at 35, 65 and 180 seconds after the injection of contrast agent (350 mg I/mL; Omnipaque, GE HealthCare) at a rate of 4 mL/s and dose of 2 mL/kg body weight.

Fusion imaging procedure

BMUS-CT/MRI fusion

Prior to fusion imaging, radiologists reviewed the patient's CT/MRI images to determine the most appropriate image for the fusion process. Artery phase and hepatobiliary specific phase images were generally preferred. The main fusion procedures were as follows: (I) the selected CT/MRI images were uploaded in Digital Imaging and Communications in Medicine (DICOM) format. (II) Real-time sonograms were registered with the uploaded CT/MRI images, including plane registration and point registration. Registration was first performed using the uniplanar method. Specific anatomical landmarks were then selected to achieve point-to-point registration. The most commonly used anatomical landmarks included portal vein bifurcation, hepatic vein, hepatic cyst, and calcification, among others. (III) Anatomical landmarks near the target lesion were selected to achieve a more precise registration. After registration, the distance between the same anatomical mark on both images was measured, and a distance <5 mm was considered to be a successful registration. (IV) The lesion was examined using multisectional scanning after the target lesion was localized by fusion imaging.

CEUS-CT/MRI fusion

A bolus of 1.2 mL of SonoVue or 0.6 mL of Sonazoid was administered, followed by a 5-mL flush of 0.9% sodium chloride solution via a peripheral venous line. We then

Figure 1 Four-point scale of lesion visibility. 1, not visible; 2, visible below 50% of the lesion border; 3, visible between 50% and 90% of the lesion border; and 4, visible above 90% of the lesion border.

observed the target lesion in real time and performed registration with the uploaded CT/MRI images. After successful registration, the contrast agent was injected again to facilitate localization of the target lesion and observation of the enhancement patterns.

Biopsy procedure

During CEUS fusion, when the lesions were at their clearest stage, all PLBs were performed by the same experienced radiologist. After routine local sterilization, draping and anesthesia, a 17-gauge trocar was inserted into the anterior margin of the tumor, with care being taken to avoid damage to the surrounding vital blood vessels and organs. An 18-gauge semiautomatic cutting needle was then passed along the trocar and placed in the central portion of the neoplasm. Needle direction was adjusted slightly during the procedure. After the biopsy tip was activated, the needle was withdrawn immediately. After the above-described procedures were repeated 2–5 times, the trocar was finally withdrawn. Local compression was applied for hemostasis. The obtained tissue was fixed in 10% formalin solution. Finally, color Doppler US was performed to detect local bleeding. An abdominal bandage was applied if no local bleeding was detected. Eating was prohibited after the biopsy. All patients were kept in bed, and their vital signs were monitored for 8 hours.

Detection rate, lesion visibility, and initial qualitative diagnosis

The detection rates of BMUS, BMUS fusion, and CEUS fusion were calculated and compared. For patients with infiltrative or multiple lesions, lesions selected for PLB were included in the calculation. Lesion visibility was graded on a four-point scale as follows: 1, not visible; 2, visible below 50% of the lesion border; 3, visible between 50% and 90% of the lesion border; and 4, visible above 90% of the lesion border (*Figure 1*). Technical success was considered to be the valid collection of the specimen. If the pathological result of the specimen obtained was consistent with the final diagnosis, the biopsy was considered a diagnostic success. Additionally, the radiologists made preliminary diagnoses of benign and malignant lesions based on the echo characteristics and enhancement patterns of the lesions during fusion imaging.

Final diagnosis and follow-up

If pathologic examination revealed specific characteristics of the neoplasm and provided accurate diagnosis, the pathological result was considered to be the final diagnosis. On the other hand, if the pathologic result of the specimen obtained was benign or negative, the final diagnosis was made by combining the results of laboratory tests and imaging findings. Follow-up was conducted in all patients for at least 6 months so that their treatment schedules could be recorded.

Data analysis

Statistical analysis was performed with a SPSS 22.0 (IBM Corp., Armonk, NY, USA). Quantitative data are presented as the mean ± standard deviation. Positive detection was defined as lesion visibility score >1. The detection rate between BMUS fusion and CEUS fusion was compared using the McNemar test. The Fisher exact test was used to compare lesion visibility. Propensity score matching analysis was performed to compare the visibility score of the nodular and infiltrative lesions. All reported P values were two-tailed. $P<0.05$ was considered statistically significant.

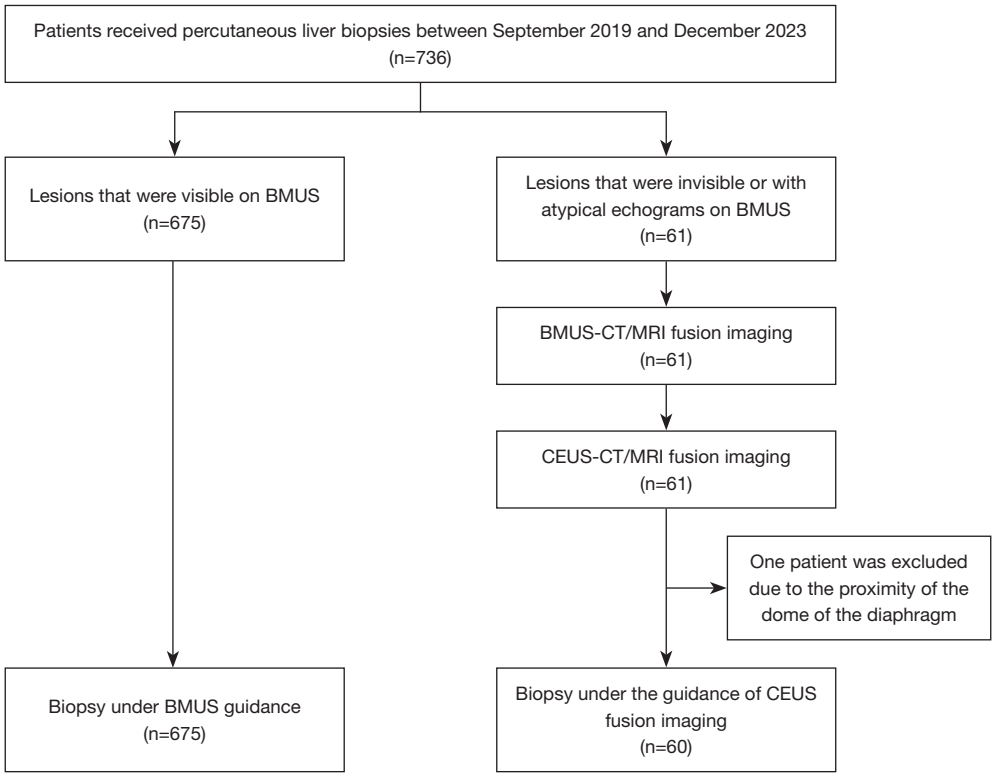

Figure 2 Flow diagram of the study. BMUS, B-mode ultrasound; CT, computed tomography; MRI, magnetic resonance imaging; CEUS, contrast-enhanced ultrasound.

Results

Baseline characteristics

The study included 61 patients (70 lesions; males: 484; females: 252; mean age: 60.2±11.5 years; age range: 34–83 years) (*Figure 2*). Fifteen patients had a history of cancer, including liver cancer (n=9), duodenal cancer (n=4), breast cancer (n=1), and pancreatic cancer (n=1). Other baseline patient characteristics are summarized in *Table 1*. The lesions in 18 patients were identified as diffuse HCC, which was defined as multiple tumors diffusely distributed in the liver lobe or liver segment without obvious margins. The baseline lesion characteristics are shown in *Table 2*.

Registration of image fusion

The registration of BMUS fusion and CEUS fusion was successfully performed in all 61 patients. Forty CT images and sixteen MRI images were uploaded for registration. No severe complication was observed during the CEUS procedure. SonoVue was used in 50 patients, Sonazoid was used in 3 patients, and 7 patients received both SonoVue and Sonazoid.

Detection rate and visibility score

The mean visibility score of 70 lesions on BMUS was 1.51±0.52. BMUS fusion detected 31 (31/70, 44.3%) lesions, achieving a mean visibility score of 1.81±1.03. CEUS fusion detected 63 (63/70, 90%) lesions, achieving a mean visibility score of 2.90±0.30. Of the 39 lesions that were invisible on BMUS fusion, CEUS fusion corrected 33 (33/39, 84.6%) of them. Our study included 30 lesions with a diameter ≤2 cm and 40 lesions with a diameter >2 cm. The comparison of their visibility scores on BMUS fusion and CEUS fusion is shown in *Table 3*. As illustrated in *Figure 3*, the value of CEUS fusion in the detection and guidance of biopsies for lesions with a diameter of less than 2 centimeters is demonstrated. Moreover, subgroup analysis was conducted in patients with nodular (n=52) and infiltrative (n=18) lesions (*Table 4*). The results indicated that CEUS fusion significantly increased the visibility score

Table 1 Patients' baseline characteristics (n=61)

Characteristic	Value
Age (years), mean ± SD [range]	60.2±11.5 [34–83]
Gender (male/female)	42/19
Liver cirrhosis (yes/no)	39/22
Hepatitis (HBV/HCV/ALD)	43/1/1
Alpha-fetoprotein (≥10 ng/mL)	34
Carcinoembryonic antigen (≥5 ng/mL)	29
Carbohydrate antigen 125 (≥35 U/mL)	20
Carbohydrate antigen 199 (≥27 U/mL)	27
Final diagnosis	
Pathology/clinical	51/10
Malignant (primary HCC/ICC/HCC recurrence/metastasis)	56 (36/8/4/8)
Benign (inflammatory nodule/HGDN/RN/ hepatic angiomatosis)	4 (1/1/1/1)
Uncertain	1

SD, standard deviation; HBV, hepatitis B virus; HCV, hepatitis C virus; ALD, autoimmune hepatitis; HCC, hepatocellular carcinoma; ICC, intrahepatic cholangiocarcinoma; HGDN, high-grade dysplastic nodule; RN, regenerative nodule.

Table 2 Baseline lesion characteristics (n=70)

Characteristic	Value
Diameter (cm), mean ± SD [range]	4.5±4.1 [0.8–18]
Lesion count	
Single	27
Multiple (2 lesions/3 lesions)	10/6
Diffuse HCCs	27
Location	
Left robe	12
Right robe	40
Diffuse HCCs	18

SD, standard deviation; HCC, hepatocellular carcinoma.

Table 3 Comparison of visibility scores for lesions of different sizes on BMUS fusion and CEUS fusion

BMUS fusion	CEUS fusion				Total
	Score 1	Score 2	Score 3	Score 4	
Total (n=70)					
Score 1	6 (8.6)	9 (12.9)	15 (8.6)	9 (12.9)	39
Score 2	0 (0.0)	4 (5.7)	5 (7.1)	2 (2.9)	11
Score 3	1 (1.4)	0 (0.0)	7 (10)	6 (8.6)	14
Score 4	0 (0.0)	0 (0.0)	3 (4.3)	3 (4.3)	6
≤2 cm (n=30)					
Score 1	0 (0.0)	1 (3.3)	7 (23.3)	8 (26.7)	16
Score 2	0 (0.0)	0 (0.0)	0 (0.0)	2 (6.7)	2
Score 3	1 (3.3)	0 (0.0)	1 (3.3)	5 (16.7)	7
Score 4	0 (0.0)	0 (0.0)	2 (6.7)	3 (10.0)	5
>2 cm (n=40)					
Score 1	6 (15.0)	8 (20.0)	8 (20)	1 (2.5)	23
Score 2	0 (0.0)	4 (10.0)	5 (12.5)	0 (0.0)	9
Score 3	0 (0.0)	0 (0.0)	6 (15.0)	1 (2.5)	7
Score 4	0 (0.0)	0 (0.0)	1 (2.5)	0 (0.0)	1

The count of lesions with different visibility scores is presented as the number (%). Score 1: not visible. Score 2: visible below 50% of the lesion border. Score 3: visible between 50% and 90% of the lesion border. Score 4: visible above 90% of the lesion border. BMUS, B-mode ultrasound; CEUS, contrast-enhanced ultrasound.

of infiltrative liver lesions (P=0.012) (*Figure 4*).

Enhancement patterns

Among the lesions, 63 were identified by CEUS fusion, of which 43 (43/63, 68.3%) appeared with hyperenhancement in the artery phase (homogeneous: 38; inhomogeneous: 8), which included ring enhancement (n=1), nodular enhancement (n=1), and patch enhancement (n=1). Moreover, 22 (22/63, 34.9%) lesions displayed rapid wash-in and rapid wash-out, while 15 (21.4%) lesions showed rapid or peripheral nodular wash-in and no wash-out. Of the 10 (15 lesions) patients who received Sonazoid, washout was observed in 13 (13/15, 86.7%) lesions in the Kupffer phase (*Table 5*).

Success rate and complications of biopsy

Among 60 patients, 72 PLB procedures under fusion

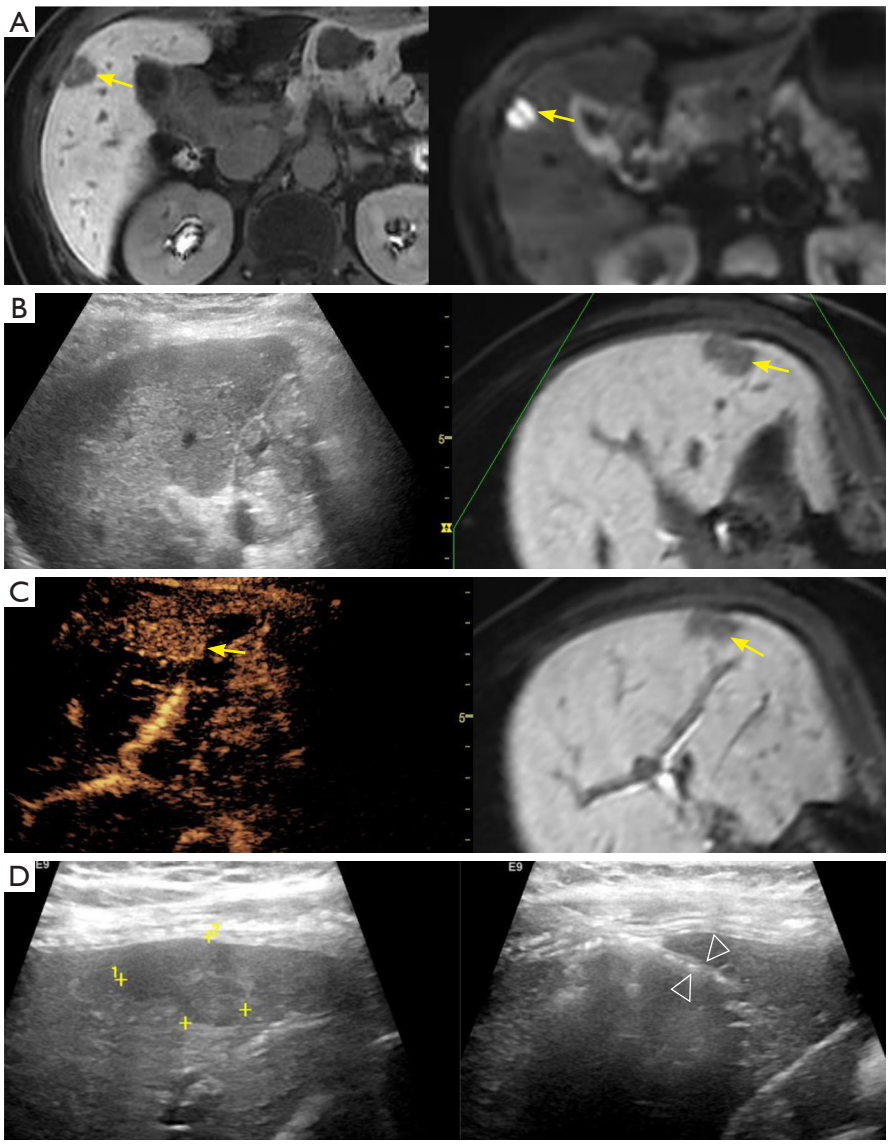

Figure 3 A-69-year-old female with a 12-year history of postoperative duodenal carcinoma. (A) A focal liver lesion (0.9 cm) detected by magnetic resonance imaging (yellow arrows: the target lesion). (B) The target lesion appeared inconspicuous on B-mode ultrasound fusion (yellow arrow: the target lesion). (C) A nodule with hyperenhancement was identified on contrast-enhanced ultrasound fusion (yellow arrows: the target lesion). (D) Biopsy was performed under the guidance of high-frequency ultrasound (white arrowheads: biopsy needle).

Table 4 Comparison of the visibility scores for nodular and infiltrative lesions on BMUS, BMUS fusion, and CEUS fusion

Imaging methods	Total cohort			PSM cohort		
	Nodular, n=52	Infiltrative, n=18	P value	Nodular, n=16	Infiltrative, n=16	P value
BMUS	1.51±0.93	1.36±0.66	0.648	1.44±0.96	1.19±0.54	0.499
BMUS fusion	1.81±1.04	1.36±0.66	0.168	2.06±1.18	1.19±0.54	0.098
CEUS fusion	2.9±0.93	2.23±0.92	0.012	3.38±0.89	2.19±0.98	0.012

The average lesion visibility score of nodular or infiltrative lesions under different imaging methods is presented as the mean ± standard deviation. BMUS, B-mode ultrasound; CEUS, contrast-enhanced ultrasound; PSM, propensity score matching.

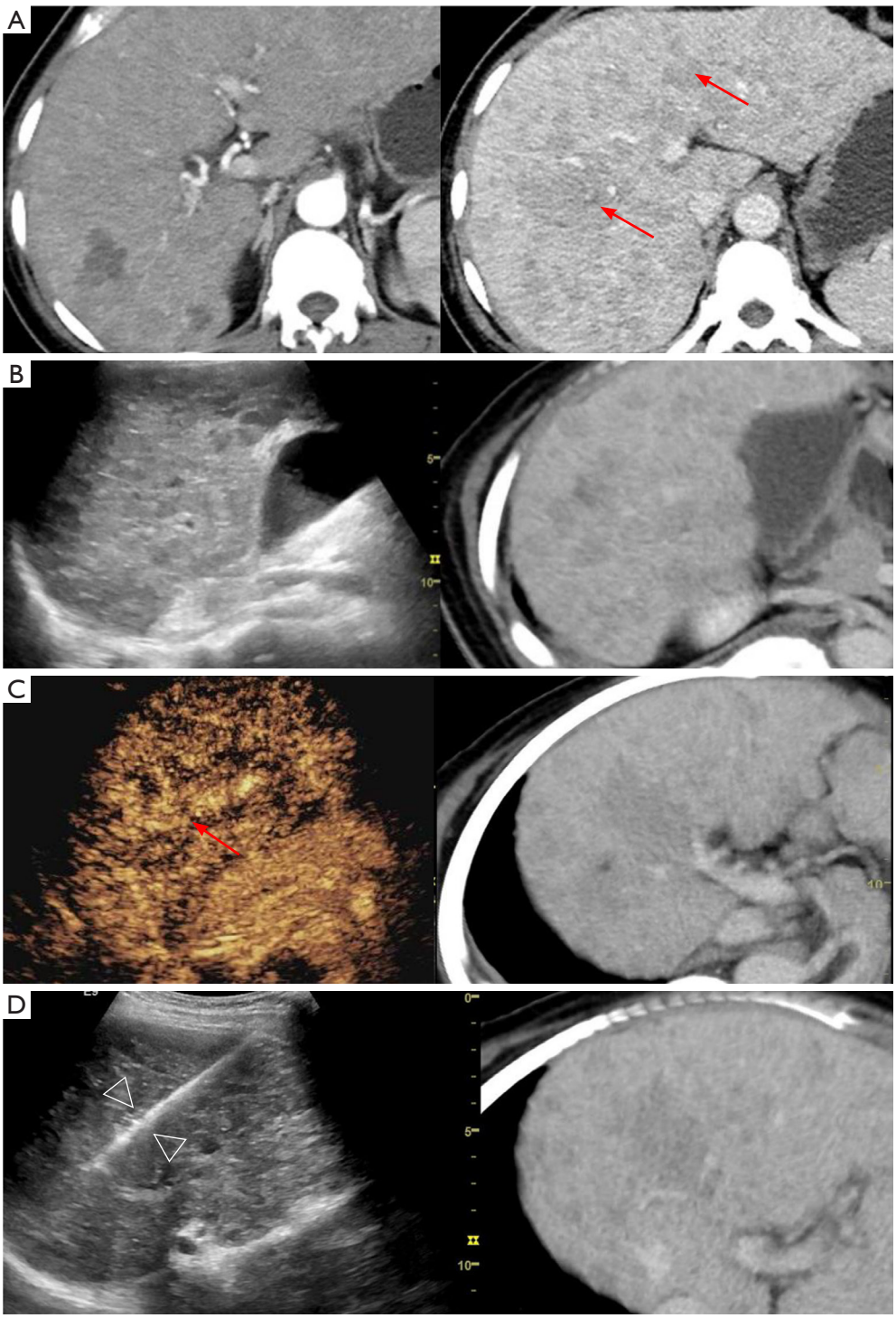

Figure 4 A 41-year-old female with HCC and bone metastasis. (A) Diffusely distributed masses revealed by contrast-enhanced computed tomography (red arrows: infiltrative HCCs). (B) Multiple heterogeneous hyperechoic zones with unclear boundaries on B-mode ultrasound fusion. (C) Masses with partial hyperenhancement identified in the artery phase of contrast-enhanced ultrasound fusion (red arrow: infiltrative HCCs). (D) B-mode ultrasound fusion-guided biopsy (white arrowheads: biopsy needle). HCC, hepatocellular carcinoma.

Table 5 The enhancement patterns of the 63 lesions visible on CEUS fusion

Phase	Count (n=63)
Artery phase	
Hyperenhancement	43
Isoenhancement	7
Hypoenhancement	13
Portal phase	
Isoenhancement	29
Hypoenhancement	34
Delay phase	
Isoenhancement	20
Hypoenhancement	43
Kupffer phase	
Isoenhancement	2
Hypoenhancement	13

CEUS, contrast-enhanced ultrasound.

Table 6 Fusion-assisted treatment schedules for 60 patients*

Prognosis	Number
Follow-up	9
Minimally invasive therapy	27
Ablation	11
PTCD	1
TACE	12
TAI	3
Comprehensive therapy	15
Other treatments	9
Hepatoprotective therapy	1
Targeted therapy	1
Chemotherapy	3
Immunotherapy	4

*, 1 patient lost to follow-up. PTCD, percutaneous transhepatic cholangial drainage; TACE, transcatheter arterial chemoembolization; TAI, transcatheter artery infusion.

guidance were completed, during which no severe complications were observe. One patient was excluded because the target lesion was located in the S7 segment and 1.2 cm from the dome of the diaphragm, which limited the percutaneous path. Three patients received the biopsy twice: (I) in one patient with suspected HCC, the first biopsy guided by CEUS (SonoVue) fusion was negative, which was considered a false negative. The result of the second biopsy guided by CEUS (Sonazoid) fusion 1 month later revealed malignancy. (II) Two biopsies were performed in one patient because the first biopsy was negative on hepatobiliary-phase MRI fusion, but the second biopsy guided by the arterial phase MRI image was positive. (III) In one patient with hyperechoic nodules, the first biopsy result indicated a cirrhosis nodule, and the second biopsy 1 month later was still negative. The lesion was considered a false-negative result based on its clinical characteristics.

Specimens were successfully obtained in 60 patients (72 cases), representing a technical success rate of 98.4% (60/61). The pathology results from 50 patients (59 specimens) were consistent with the final diagnosis, representing a diagnostic success rate of 82.0% (50/63). No malignant cells were found in 12 specimens: (I) based on laboratory tests and imaging results, 9 specimens were identified as false negatives, including 2 lesions that proved positive on follow-up biopsies. (II) Two specimens obtained were negative because US showed fewer lesions than did MRI. (III) The diagnosis of 1 lesion was unclear because the biopsy result showed hepatic angiomatosis, while the MRI result indicated liver metastasis.

Final diagnoses and prognoses

The final diagnosis of 50 patients was based on the pathological results from CEUS fusion-guided PLB. The final diagnosis of 11 patients was determined through the consideration of both the pathological results and their clinical characteristics. The final diagnoses for 61 patients are listed in *Table 1*. Experienced sonographers preliminarily diagnosed 5 benign lesions and 54 malignant lesions based on the echo characteristics and enhancement patterns during CEUS fusion imaging. With final diagnosis as the gold standard, the use of CEUS fusion achieved a sensitivity of 96.3%, an accuracy of 93.1%, a specificity of 50.0%, a positive predictive value of 96.3%, and a negative predictive value of 50%. *Table 6* shows the fusion-assisted treatment schedules for 61 patients.

Discussion

Conventional BMUS is the primary imaging method for the screening and diagnosis of FLLs. However, the single

acoustic window has the potential to limit the resolution, particularly in the case of rough liver echo texture, which may result in the misdiagnosis of certain lesions (25). The advent of precision medicine has necessitated the exploration of novel imaging techniques that can overcome the limitations of traditional US. As a supplementary examination following BMUS, CEUS vastly improves the detection and qualitative diagnosis of FLLs, with a diagnostic accuracy for HCC inconspicuous on BMUS reaching 93.8% to 100%. This diagnostic accuracy is comparable to that of CECT or CEMRI (26-28). Furthermore, the development of fusion imaging technology enables the combination of CT/MRI images and real-time US images for the accurate localization lesions that may be missed by conventional US scanning (29). Consequently, the integration of CEUS and fusion imaging technology can concurrently address the localization and preliminary diagnosis of lesions that are undetectable by conventional BMUS.

Our study compared BMUS fusion and CEUS fusion in terms of their detection rate for BMUS-invisible lesions. The results demonstrated that the visibility score and detection rate of BMUS-invisible lesions of CEUS fusion were significantly superior to those of BMUS fusion (P<0.001). The combination of fusion imaging with CEUS significantly enhanced lesion localization and the surrounding tissue contrast, thereby improving the detection of lesions that were previously undetectable by BMUS due to echo or location. The value of CEUS fusion in the detection of lesions with poor conspicuity on BMUS has been corroborated by several previous studies (30-33).

For malignant nodules, such as small HCC, the early detection and biopsy with pathological confirmation are critical to the treatment and prognosis of patients. However, the limited spatial resolution of BMUS may result in the misdiagnosis of small HCC, thereby precluding the opportunity for PLB and US-guided interventional therapy for these lesions. Our study demonstrated the value of CEUS fusion in the detection and biopsy guidance of invisible lesions <2 cm in size on BMUS. Fusion imaging can facilitate the identification of small-sized lesions that BMUS may fail to detect (34). Numerous studies have demonstrated the advantages of fusion imaging in the detection of small lesions with a diameter of less than 10 mm (35). In a study by Lee *et al.*, it was found that fusion imaging was significantly more effective than was BMUS in the detection of HCCs smaller than 2.0 cm (P<0.001) (25). Furthermore, Zhou *et al.* demonstrated that the detection rates of CEUS alone and CEUS fusion in 68 liver lesions with a diameter of ≤1 cm were 71.4% and 95.6%, respectively (P<0.001) (36), which also proved the superiority of CEUS fusion over CEUS alone in the detection of small lesions.

Infiltrative HCC typically presents as small neoplasms that disseminate throughout the liver or specific segment/lobe (37). The lack of clearly defined boundaries and the occurrence in the liver cirrhosis background present a challenge in the identification of infiltrative HCC. In our study, 18 patients with infiltrative HCC or intrahepatic cholangiocarcinoma (ICC) exhibited consistently low mean visibility scores on both BMUS and BMUS fusion, which were significantly improved after CEUS fusion, with a biopsy success rate of 100% (18/18) achieved under CEUS fusion guidance. The subgroup analysis of nodular lesions and infiltrative lesions also demonstrated the superiority of CEUS fusion in enhancing the visibility score of infiltrative lesions (P=0.012). Early detection is vital to the treatment and prognosis of patients with infiltrative HCC, given the advanced stage and the poor prognosis associated with vascular invasion in the first treatment (38-40). Our results support the clinically significant value of CEUS fusion in the early detection of infiltrative HCC.

Currently, the application of CEUS fusion primarily related RFA and includes preablation range assessment, intra-ablation guidance, and local progression and recurrence rate after ablation (41-44). Several studies have combined 3D imaging with CEUS fusion to evaluate the postablation edge, with the findings indicating that 3D-CEUS fusion has superior automaticity and advantages in the evaluation of postablation edges as compared two-dimensional imaging, while providing a shortened registration time (45-50). However, there has been a paucity of research on the value of CEUS fusion in PLB. Studies have demonstrated that BMUS fusion can achieve a higher rate of technical success and diagnostic success in PLB (51-53). With regard to the use of CEUS fusion in PLB, Kang *et al.* demonstrated that CEUS fusion can achieve a higher rate of technical success in PLB in comparison to BMUS fusion (26,54). Our findings indicate that CEUS fusion can not only improve the lesion detection and operator's confidence so as to increase the technical success rate of PLB but can also assist sonographers in the preliminary diagnosis of benign and malignant lesions and obtain a high rate of diagnostic success in PLB.

Although the majority of BMUS-invisible lesions were detected after CEUS fusion, seven lesions remained undetected, including five cases of infiltrative HCC. Although the literature indicates that the use of fusion imaging can enhance the detection rate of lesions and improve patient satisfaction, its application may be constrained by a number of factors (55,56). First, unavoidable diaphragmatic breathing and respiratory movements can cause incorrect registration for lesions that are located under the diaphragm or in the peripheral liver remote to the great vessels. Second, Lim *et al.* (23) reported that even if the target hepatic lesion is clearly visualized on fusion imaging, there is still a chance of inaccurate localization of the target lesion during the biopsy procedure or RFA. For instance, an abnormal perfusion area can be mistaken for the target lesion during a biopsy procedure, resulting in a false-negative result. Third, landmark-based nonrigid registration was used in our study since the liver is a nonrigid organ. Although this method can restrict the partial influence of liver motion, its computation is complex and time-consuming, making the realization of real-time imaging challenging (57).

It is worth noting that devices equipped with US fusion imaging technology are generally more expensive than are conventional US diagnostic devices. They require the integration of more advanced hardware and software to achieve multimodal image fusion and real-time navigation and involve more complex technologies, including real-time 3D imaging and digital beamforming (58). However, numerous clinical studies have demonstrated that the novel approach of using preoperative MRI/CT images and intraoperative or postoperative US image fusion guidance during interventional procedures not only ensures the real-time guidance of US but also guarantees the accuracy of guidance due to the incorporation of preoperative MRI/CT images (6,31,44,59). Therefore, despite the challenges in expenses associated with US fusion imaging technology, it holds potential in improving therapeutic outcomes and reducing long-term healthcare costs. To broaden its application in regions with limited medical resources, it is necessary to reduce the cost of devices, enhance the intelligence and portability of the devices, and strengthen the professional training of sonologists.

Conclusions

In conclusion, our study demonstrated that the use of CEUS fusion for guiding the PLB of lesions invisible on BMUS can significantly enhance the visibility score and the detection, thereby improving the biopsy success rate, particularly in cases of infiltrative HCC and small HCC (<2 cm). However, certain limitations were associated with our study. First, we employed a single-center, retrospective design, and thus the findings may not be generalizable. Further studies with larger sample sizes are needed to confirm these results. Secondly, the study included only one group and lacked a comparison of biopsy success rates for CEUS, BMUS fusion, and CEUS fusion. Future studies could combine 3D imaging technology with CEUS fusion to provide the clearest image guidance for BMUS-invisible lesions during US-guided interventional therapies.

Acknowledgments

None.

Footnote

Reporting Checklist: The authors have completed the STROBE reporting checklist. Available at https://qims.amegroups.com/article/view/10.21037/qims-24-1104/rc

Funding: This study received funding from the Nanjing Drum Tower Hospital Clinical Trial Special Fund Projects of 2022.

Conflicts of Interest: All authors have completed the ICMJE uniform disclosure form (available at https://qims.amegroups.com/article/view/10.21037/qims-24-1104/coif). The authors have no conflicts of interest to declare.

Ethical Statement: The authors are accountable for all aspects of the work in ensuring that questions related to the accuracy or integrity of any part of the work are appropriately investigated and resolved. This study was conducted in accordance with the Declaration of Helsinki (as revised in 2013) and was approved by the Institutional Ethics Committee of the Nanjing Drum Tower Hospital, Affiliated Hospital of Medical School, Nanjing University (No. 2022-140-01). Informed consent were obtained from all the patients.

References

1. Lim S, Kim YK, Park HJ, Lee WJ, Choi D, Park MJ. Infiltrative hepatocellular carcinoma on gadoxetic acid-enhanced and diffusion-weighted MRI at 3.0T. J Magn Reson Imaging 2014;39:1238-45.
2. Marin D, Furlan A, Federle MP, Midiri M, Brancatelli G. Imaging approach for evaluation of focal liver lesions. Clin Gastroenterol Hepatol 2009;7:624-34.
3. Salarian M, Turaga RC, Xue S, Nezafati M, Hekmatyar K, Qiao J, et al. Early detection and staging of chronic liver diseases with a protein MRI contrast agent. Nat Commun 2019;10:4777.
4. Zhou IY, Catalano OA, Caravan P. Advances in functional and molecular MRI technologies in chronic liver diseases. J Hepatol 2020;73:1241-54.
5. Jolesz FA, Hynynen K, McDannold N, Freundlich D, Kopelman D. Noninvasive thermal ablation of hepatocellular carcinoma by using magnetic resonance imaging-guided focused ultrasound. Gastroenterology 2004;127:S242-7.
6. Minami Y, Okumura N, Yamamoto N, Tsuji N, Kono Y, Kudo M. Quantification of tumor vascularity with contrast-enhanced ultrasound for early response of transcatheter arterial chemoembolization for hepatocellular carcinoma: a report of three cases. J Med Ultrason (2001) 2012;39:15-9.
7. Jiang HY, Chen J, Xia CC, Cao LK, Duan T, Song B. Noninvasive imaging of hepatocellular carcinoma: From diagnosis to prognosis. World J Gastroenterol 2018;24:2348-62.
8. Smith EA, Grove JJ, Van Der Spek AFL, Jarboe MD. Magnetic-resonance-guided biopsy of focal liver lesions. Pediatr Radiol 2017;47:750-4.
9. Hoffmann P, Cyrany J, Kopecky J, Hoffmannova M, Ryska P, Hulek M, Dvorak P. Percutaneous CT-guided Biopsy of Focal Liver Lesions - Long- term Experience with more than 300 Procedures. J Gastrointestin Liver Dis 2023;32:197-205.
10. Kudo M, Ueshima K, Osaki Y, Hirooka M, Imai Y, Aso K, Numata K, Kitano M, Kumada T, Izumi N, Sumino Y, Ogawa C, Akazawa K. B-Mode Ultrasonography versus Contrast-Enhanced Ultrasonography for Surveillance of Hepatocellular Carcinoma: A Prospective Multicenter Randomized Controlled Trial. Liver Cancer 2019;8:271-80.
11. Liu F, Liu D, Wang K, Xie X, Su L, Kuang M, Huang G, Peng B, Wang Y, Lin M, Tian J, Xie X. Deep Learning Radiomics Based on Contrast-Enhanced Ultrasound Might Optimize Curative Treatments for Very-Early or Early-Stage Hepatocellular Carcinoma Patients. Liver Cancer 2020;9:397-413.
12. Francica G, Meloni MF, de Sio I, Terracciano F, Caturelli E, Riccardi L, Roselli P, Iadevaia MD, Scaglione M, Lenna G, Chiang J, Pompili M. Biopsy of Liver Target Lesions under Contrast-Enhanced Ultrasound Guidance - A Multi-Center Study. Ultraschall Med 2018;39:448-53.
13. Shi H, Ong YT, Gogna A, Venkatanarasimha N, Sanamandra SK, Leong S, Irani FG, Lo RHG, Too CW. Perfluorobutane contrast-enhanced ultrasonography: a new standard for ultrasonography-guided thermal ablation of sonographically occult liver tumours? Singapore Med J 2021;62:546-53.
14. Tzartzeva K, Obi J, Rich NE, Parikh ND, Marrero JA, Yopp A, Waljee AK, Singal AG. Surveillance Imaging and Alpha Fetoprotein for Early Detection of Hepatocellular Carcinoma in Patients With Cirrhosis: A Meta-analysis. Gastroenterology 2018;154:1706-1718.e1.
15. Wu W, Chen MH, Yan K, Yin SS, Dai Y, Fan ZH, Yang W, Li JY. Application of contrast-enhanced ultrasound to increase the diagnostic rate of liver tumor by biopsy. Zhonghua Yi Xue Za Zhi 2006;86:116-20.
16. Krücker J, Xu S, Venkatesan A, Locklin JK, Amalou H, Glossop N, Wood BJ. Clinical utility of real-time fusion guidance for biopsy and ablation. J Vasc Interv Radiol 2011;22:515-24.
17. Tang A, Bashir MR, Corwin MT, Cruite I, Dietrich CF, Do RKG, Ehman EC, Fowler KJ, Hussain HK, Jha RC, Karam AR, Mamidipalli A, Marks RM, Mitchell DG, Morgan TA, Ohliger MA, Shah A, Vu KN, Sirlin CB; . Evidence Supporting LI-RADS Major Features for CT- and MR Imaging-based Diagnosis of Hepatocellular Carcinoma: A Systematic Review. Radiology 2018;286:29-48.
18. Afif AM, Laroco OD, Lau S, Teo SM, Rahman AA, Too CW, Venkatanarasimha N, Gogna A. Usefulness of ultrasound fusion technology for hepatocellular carcinoma localisation, pre- and post-thermal ablation. Ultrasound 2022;30:194-200.
19. Bo XW, Xu HX, Wang D, Guo LH, Sun LP, Li XL, Zhao CK, He YP, Liu BJ, Li DD, Zhang K. Fusion imaging of

contrast-enhanced ultrasound and contrast-enhanced CT or MRI before radiofrequency ablation for liver cancers. Br J Radiol 2016;89:20160379.
20. Calandri M, Ruggeri V, Carucci P, Mirabella S, Veltri A, Fonio P, Gazzera C. Thermal ablation with fusion imaging guidance of hepatocellular carcinoma without conspicuity on conventional or contrast-enhanced US: surrounding anatomical landmarks matter. Radiol Med 2019;124:1043-8.
21. Lee DH, Lee JM. Recent Advances in the Image-Guided Tumor Ablation of Liver Malignancies: Radiofrequency Ablation with Multiple Electrodes, Real-Time Multimodality Fusion Imaging, and New Energy Sources. Korean J Radiol 2018;19:545-59.
22. Lee MW. Fusion imaging of real-time ultrasonography with CT or MRI for hepatic intervention. Ultrasonography 2014;33:227-39.
23. Lim S, Lee MW, Rhim H, Cha DI, Kang TW, Min JH, Song KD, Choi SY, Lim HK. Mistargeting after fusion imaging-guided percutaneous radiofrequency ablation of hepatocellular carcinomas. J Vasc Interv Radiol 2014;25:307-14.
24. Lee MW, Rhim H, Cha DI, Kim YJ, Lim HK. Planning US for percutaneous radiofrequency ablation of small hepatocellular carcinomas (1-3 cm): value of fusion imaging with conventional US and CT/MR images. J Vasc Interv Radiol 2013;24:958-65.
25. Lee MW, Lim HK, Kim YJ, Choi D, Kim YS, Lee WJ, Cha DI, Park MJ, Rhim H. Percutaneous sonographically guided radio frequency ablation of hepatocellular carcinoma: causes of mistargeting and factors affecting the feasibility of a second ablation session. J Ultrasound Med 2011;30:607-15.
26. Kang TW, Lee MW, Song KD, Kim M, Kim SS, Kim SH, Ha SY. Added Value of Contrast-Enhanced Ultrasound on Biopsies of Focal Hepatic Lesions Invisible on Fusion Imaging Guidance. Korean J Radiol 2017;18:152-61.
27. Korenaga K, Korenaga M, Furukawa M, Yamasaki T, Sakaida I. Usefulness of Sonazoid contrast-enhanced ultrasonography for hepatocellular carcinoma: comparison with pathological diagnosis and superparamagnetic iron oxide magnetic resonance images. J Gastroenterol 2009;44:733-41.
28. Wei Y, Ye Z, Yuan Y, Huang Z, Wei X, Zhang T, Wan S, Tang H, He X, Song B. A New Diagnostic Criterion with Gadoxetic Acid-Enhanced MRI May Improve the Diagnostic Performance for Hepatocellular Carcinoma. Liver Cancer 2020;9:414-25.
29. Ewertsen C, Henriksen BM, Torp-Pedersen S, Bachmann Nielsen M. Characterization by biopsy or CEUS of liver lesions guided by image fusion between ultrasonography and CT, PET/CT or MRI. Ultraschall Med 2011;32:191-7.
30. Beutler BD, Whang G, Tchelepi H. PET/CT Ultrasound Fusion for Percutaneous Biopsy: A Retrospective Single-Center Study and Review of the Literature. Clin Nucl Med 2022;47:692-8.
31. Minami Y, Kudo M. Image Guidance in Ablation for Hepatocellular Carcinoma: Contrast-Enhanced Ultrasound and Fusion Imaging. Front Oncol 2021;11:593636.
32. Kloth C, Kratzer W, Schmidberger J, Beer M, Clevert DA, Graeter T. Ultrasound 2020 - Diagnostics & Therapy: On the Way to Multimodal Ultrasound: Contrast-Enhanced Ultrasound (CEUS), Microvascular Doppler Techniques, Fusion Imaging, Sonoelastography, Interventional Sonography. Rofo 2021;193:23-32.
33. Gennaro N, Schiaffino S, Mauri G, Monfardini L. The What, the Why, and the How of Liver Ablations: A Practical Guide for the Medical Oncologist. Oncology 2021;99:722-31.
34. Okamoto E, Sato S, Sanchez-Siles AA, Ishine J, Miyake T, Amano Y, Kinoshita Y. Evaluation of virtual CT sonography for enhanced detection of small hepatic nodules: a prospective pilot study. AJR Am J Roentgenol 2010;194:1272-8.
35. Song KD, Lee MW, Rhim H, Kang TW, Cha DI, Sinn DH, Lim HK. Percutaneous US/MRI Fusion-guided Radiofrequency Ablation for Recurrent Subcentimeter Hepatocellular Carcinoma: Technical Feasibility and Therapeutic Outcomes. Radiology 2018;288:878-86.
36. Zhou Y, Wang Y, Wang F, Zhang X, Ding J, Zhou H, Jing X. Additional Diagnostic Value of Fusion Imaging of CEUS and First CEUS of Invisible Hepatic Lesions ≤2 cm. J Ultrasound Med 2021;40:1173-81.
37. Madani SP, Mirza-Aghazadeh-Attari M, Mohseni A, Pawlik T, Kamel IR. Diffuse infiltrative hepatocellular carcinoma: Multimodality imaging manifestations. J Surg Oncol 2023;127:385-93.
38. Dendy MS, Camacho JC, Ludwig JM, Krasinskas AM, Knechtle SJ, Kim HS. Infiltrative Hepatocellular Carcinoma With Portal Vein Tumor Thrombosis Treated With a Single High-Dose Y90 Radioembolization and Subsequent Liver Transplantation Without a Recurrence. Transplant Direct 2017;3:e206.
39. Nisiewicz MJ, Kapoor H, Fowler KJ, Furlan A, Dugan

AJ, Owen JW. Improved survival following transarterial radioembolization of infiltrative-appearance hepatocellular carcinoma. Abdom Radiol (NY) 2021;46:1958-66.
40. Vernuccio F, Porrello G, Cannella R, Vernuccio L, Midiri M, Giannitrapani L, Soresi M, Brancatelli G. Benign and malignant mimickers of infiltrative hepatocellular carcinoma: tips and tricks for differential diagnosis on CT and MRI. Clin Imaging 2021;70:33-45.
41. Bo XW, Xu HX, Guo LH, Sun LP, Li XL, Zhao CK, He YP, Liu BJ, Li DD, Zhang K, Wang D. Ablative safety margin depicted by fusion imaging with post-treatment contrast-enhanced ultrasound and pre-treatment CECT/CEMRI after radiofrequency ablation for liver cancers. Br J Radiol 2017;90:20170063.
42. Huang Q, Zeng Q, Long Y, Tan L, Zheng R, Xu E, Li K. Fusion imaging techniques and contrast-enhanced ultrasound for thermal ablation of hepatocellular carcinoma - A prospective randomized controlled trial. Int J Hyperthermia 2019;36:1207-15.
43. Ma QP, Xu EJ, Zeng QJ, Su ZZ, Tan L, Chen JX, Zheng RQ, Li K. Intraprocedural computed tomography/magnetic resonance-contrast-enhanced ultrasound fusion imaging improved thermal ablation effect of hepatocellular carcinoma: Comparison with conventional ultrasound. Hepatol Res 2019;49:799-809.
44. Xu E, Long Y, Li K, Zeng Q, Tan L, Luo L, Huang Q, Zheng R. Comparison of CT/MRI-CEUS and US-CEUS fusion imaging techniques in the assessment of the thermal ablation of liver tumors. Int J Hyperthermia 2019;35:159-67.
45. Ding J, Wang D, Zhou Y, Zhao L, Zhou H, Jing X, Wang Y. A novel mono-modality fusion imaging method based on three-dimensional contrast-enhanced ultrasound for the evaluation of ablation margins after microwave ablation of hepatocellular carcinoma. J Gastrointest Oncol 2021;12:184-95.
46. Long H, Zhou X, Zhang X, Ye J, Huang T, Cong L, Xie X, Huang G. 3D fusion is superior to 2D point-to-point contrast-enhanced US to evaluate the ablative margin after RFA for hepatocellular carcinoma. Eur Radiol 2024;34:1247-57.
47. Xu EJ, Lv SM, Li K, Long YL, Zeng QJ, Su ZZ, Zheng RQ. Immediate evaluation and guidance of liver cancer thermal ablation by three-dimensional ultrasound/contrast-enhanced ultrasound fusion imaging. Int J Hyperthermia 2018;34:870-6.
48. Ye J, Huang G, Zhang X, Xu M, Zhou X, Lin M, Xie X, Xie X. Three-dimensional contrast-enhanced ultrasound fusion imaging predicts local tumor progression by evaluating ablative margin of radiofrequency ablation for hepatocellular carcinoma: a preliminary report. Int J Hyperthermia 2019;36:55-64.
49. You Y, Zhang M, Li K, Zeng Q, Luo L, Long Y, Tan L, He X, Liang P, Xu E, Zheng R. Feasibility of 3D US/CEUS-US/CEUS fusion imaging-based ablation planning in liver tumors: a retrospective study. Abdom Radiol (NY) 2021;46:2865-74.
50. Zhang X, Huang G, Ye J, Xu M, Cong L, He X, Huang T, Kuang M, Xie X. 3-D Contrast-Enhanced Ultrasound Fusion Imaging: A New Technique to Evaluate the Ablative Margin of Radiofrequency Ablation for Hepatocellular Carcinoma. Ultrasound Med Biol 2019;45:1933-43.
51. Park HJ, Lee MW, Lee MH, Hwang J, Kang TW, Lim S, Rhim H, Lim HK. Fusion imaging-guided percutaneous biopsy of focal hepatic lesions with poor conspicuity on conventional sonography. J Ultrasound Med 2013;32:1557-64.
52. Aj L, Kalra N, Bhatia A, Srinivasan R, Gulati A, Kapoor R, Gupta V, Dhiman RK, Chawla Y, Khandelwal N. Fusion Image-Guided and Ultrasound-Guided Fine Needle Aspiration in Patients With Suspected Hepatic Metastases. J Clin Exp Hepatol 2019;9:547-53.
53. Ahn SJ, Lee JM, Chang W, Lee SM, Kang HJ, Yang HK, Han JK. Clinical utility of real-time ultrasound-multimodality fusion guidance for percutaneous biopsy of focal liver lesions. Eur J Radiol 2018;103:76-83.
54. Kang HJ, Kim JH, Lee SM, Yang HK, Ahn SJ, Han JK. Additional value of contrast-enhanced ultrasonography for fusion-guided, percutaneous biopsies of focal liver lesions: prospective feasibility study. Abdom Radiol (NY) 2018;43:3279-87.
55. Ahmed Y, Novak RD, Nakamoto D, Azar N. Is Ultrasound Fusion a Reasonable Replacement for Computed Tomography in Guiding Abdominal Interventions? J Ultrasound Med 2016;35:1131-41.
56. Hakime A, Barah A, Deschamps F, Farouil G, Joskin J, Tselikas L, Auperin A, de Baere T. Prospective comparison of freehand and electromagnetic needle tracking for US-guided percutaneous liver biopsy. J Vasc Interv Radiol 2013;24:1682-9.
57. Dong C, Chen YW, Seki T, Inoguchi R, Lin CL, Han XH. Non-rigid image registration with anatomical structure constraint for assessing locoregional therapy of hepatocellular carcinoma. Comput Med Imaging Graph 2015;45:75-83.

58. Abdominal applications of ultrasound fusion imaging technique: liver, kidney, and pancreas. Insights Imaging 2019;10:6.
59. Minami T, Minami Y, Chishina H, Arizumi T, Takita M, Kitai S, Yada N, Inoue T, Hagiwara S, Ueshima K, Nishida N, Kudo M. Combination guidance of contrast-enhanced US and fusion imaging in radiofrequency ablation for hepatocellular carcinoma with poor conspicuity on contrast-enhanced US/fusion imaging. Oncology 2014;87 Suppl 1:55-62.

Cite this article as: He Y, Gong L, Wu J, Wen B, Kong W. The value of contrast-enhanced ultrasound fusion imaging in percutaneous liver biopsy for liver lesions invisible on conventional B-mode ultrasound. Quant Imaging Med Surg 2025;15(2):1528-1542. doi: 10.21037/qims-24-1104